

The Lack of HONO Measurement May Affect the Accurate Diagnosis of Ozone Production Sensitivity

Pengfei Liu, Chaoyang Xue, Can Ye, Chengtang Liu, Chenglong Zhang, Jinhe Wang, Yuanyuan Zhang, Junfeng Liu, and Yujing Mu*



Cite This: *ACS Environ. Au* 2023, 3, 18–23



Read Online

ACCESS |

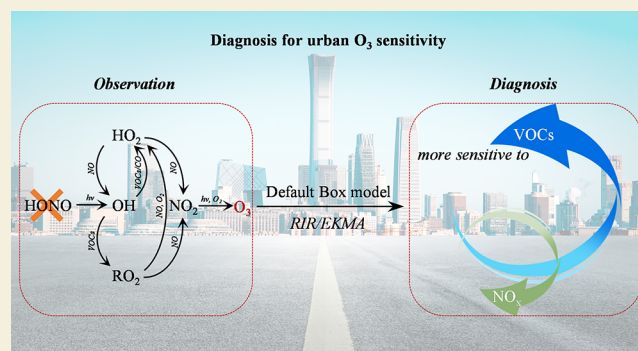
Metrics & More

Article Recommendations

Supporting Information

ABSTRACT: Recently, deteriorating ozone (O_3) pollution in China brought the precise diagnosis of O_3 sensitive chemistry to the forefront. As a dominant precursor of OH radicals, atmospheric nitrous acid (HONO) plays an important role in O_3 production. However, its measurement unavailability in many regions especially for second- and third-tier cities may lead to the misjudgment of the O_3 sensitivity regime derived from observation-based models. Here, we systematically assess the potential impact of HONO on diagnosing the sensitivity of O_3 production using a 0-dimension box model based on a comprehensive summer urban field campaign. The results indicated that the default mode (only the $NO + OH$ reaction is included) in the model could underestimate $\sim 87\%$ of observed HONO levels, leading to an obvious decrease ($\sim 19\%$) of net O_3 production in the morning, which was in line with the previous studies. The unconstrained HONO in the model was found to significantly push O_3 production toward the VOC-sensitive regime. Additionally, it is unrealistic to change NO_x but constrain HONO in the model due to the dependence of HONO formation on NO_x . Assuming that HONO varied proportionally with NO_x , a stronger NO_x -sensitive condition could be achieved. Therefore, effective reduction of NO_x should be given more attention together with VOC emission control for O_3 mitigation.

KEYWORDS: O_3 pollution, one city for one policy, HONO, sensitivity regime, RIR, EKMA



INTRODUCTION

China is currently suffering from worsening ground-level O_3 pollution, which has attracted great attention from the public due to its adverse impact on the ecosystem and human health.^{1–3} To reverse the increase in ground-level O_3 , the Ministry of Ecology and Environment of China recently announced the “one city for one policy” initiative for 54 key polluted cities in the North China Plain (NCP), the Fenwei Plain, and their surrounding areas, which drove professional scientific research teams to enter the appointed cities for alleviating O_3 pollution and improving air quality. In order to achieve the goal, it is of pivotal importance to diagnose precisely the sensitivity of O_3 production.

It is well-known that ground-level O_3 is generated from photochemical reactions involving NO_x and volatile organic compounds (VOCs).^{4,5} Unlike other air pollutants that are from secondary formation, the O_3 responses to its precursors (NO_x and VOCs) are nonlinear,^{6–8} which heightens the difficulty of formulating policies to control O_3 pollution. According to the comprehensive field measurement data and 0-dimension box model, several observation-based methods (OBMs) such as relative incremental reactivity (RIR) and empirical kinetic modeling approach (EKMA) have been

commonly developed to determine the O_3 - NO_x -VOC sensitivity.^{9–12} To restore the real atmospheric photochemical condition, most key meteorological parameters, photolysis rate constants (e.g., $J(NO_2)$), and gaseous pollutants (e.g., nitrous acid (HONO) and formaldehyde) should be strictly constrained in the 0-dimension box model.^{10,11} However, the field measurements related to these key species are lacking at present in many regions of China, especially for second- and third-tier cities that are experiencing heavy O_3 pollution.

Many studies have proposed that atmospheric HONO acting as a dominant precursor of OH radicals^{13–15} makes a great contribution to O_3 formation,^{16–18} whereas its sources are not fully understood.^{19,20} As a result, HONO formation in the default box model was only regarded to be from the homogeneous reaction of NO with OH radicals,^{21,22} leading to a visible underestimation of HONO levels. Although the gap

Received: August 22, 2022

Revised: October 10, 2022

Accepted: October 11, 2022

Published: October 13, 2022



between simulated and observed HONO concentrations could be significantly narrowed through incorporating other known sources including direct emission, heterogeneous conversion of NO_2 , and so on into the model,^{15,21,22} some key HONO-related kinetic parameters in the model are often changed optionally in order to be closer to the observation. For example, the uptake coefficient of NO_2 on surfaces could vary from 2×10^{-7} to 1×10^{-5} .^{23–25} Therefore, the high uncertainties of the HONO simulation in the box model highlighted the significance of the HONO observation-based constraint. However, to our knowledge, continuous HONO measurements in China were mostly performed in megacities such as Beijing,^{20,26–28} Shanghai,^{29–32} Guangzhou,^{33–35} and Hong Kong^{36–38} at present, and only a few focused on the second- and third-tier cities (e.g., Chengdu, Tai'an, Ji'nan, Baoding) during the summer O_3 pollution period.^{18,22,39} The absence of HONO observation not only influences the evaluation of atmospheric oxidation capacity,¹⁹ but also is likely to provide a misleading diagnosis for O_3 sensitivity regimes. Although the effect of initial HONO on the sensitivity of O_3 production in Los Angeles was preliminarily assessed in 1982 based on a simplified trajectory model,⁴⁰ the accuracy of HONO measurement and the understanding of chemical mechanisms at that time are outdated. In addition, the localization of model parameters (e.g., OBM) is also a key factor that determines computational results to some extent. Consequently, systematically assessing the role of HONO in diagnosing the sensitivity of O_3 production at present has great significance for O_3 efficient control in many Chinese cities suffering from serious O_3 pollution.

In this study, a comprehensive field campaign was performed in a typical urban site (Tai'an) of the NCP during the summer of 2018, and the impacts of atmospheric HONO on the O_3 budget and O_3 - NO_x -VOC sensitivity regime were explicitly explored to provide some insights for O_3 control strategies based on the sensitivity tests in a photochemical box model.

MATERIALS AND METHODS

Field Campaign

A comprehensive field campaign was conducted from June 16 to July 6, 2018 in Tai'an (36.18° N, 117.11° E), Shandong Province.^{22,41,42} Measurements including O_3 , NO, NO_2 , CO, SO_2 , HONO, H_2O_2 , non-methane hydrocarbon (NMHCs), oxygenated volatile organic compounds (OVOCs), peroxyacetyl nitrate (PAN), meteorological parameters (ambient temperature (T), relative humidity (RH), and atmospheric pressure (P)), and $\text{J}(\text{NO}_2)$ have been described in detail in Section S1 of the Supporting Information (SI).

Observation-Based Model

The Framework for 0-dimension Atmospheric Modeling (F0AM)⁴³ coupled with Master Chemical Mechanisms (MCM v3.3.1) was used to explore the influence of HONO on O_3 sensitive chemistry. The model was constrained by the observed meteorological parameters (T, RH, and P), $\text{J}(\text{NO}_2)$, and trace gases (NO_x family, CO, SO_2 , H_2O_2 , NMHCs, OVOCs, and PAN). Detailed information about model configuration is presented in Section S2 of the SI.

Empirical Kinetic Modeling Approach

Based on the F0AM simulations, a set of sensitivity tests for NO_x and VOCs with 49 different combinations (i.e., 1, 5, 10, 20, 50, 100, and 150% for NO_x and VOCs, respectively) were conducted to generate the EKMA contour plot. The role of HONO in the O_3 sensitivity regime was assessed by several different scenarios of EKMA that involved constrained or unconstrained HONO. Note that unconstrained HONO meant the measured HONO concentrations were not input in the model. For more details, see Section S3 of the SI.

RESULTS AND DISCUSSION

Overview of the Field Observations and O_3 Budget

The temporal variations of O_3 and relevant key parameters ($\text{J}(\text{NO}_2)$, T, NO_x , HONO, NMHCs, and OVOCs) for the entire observation period are illustrated in Figure 1, and their

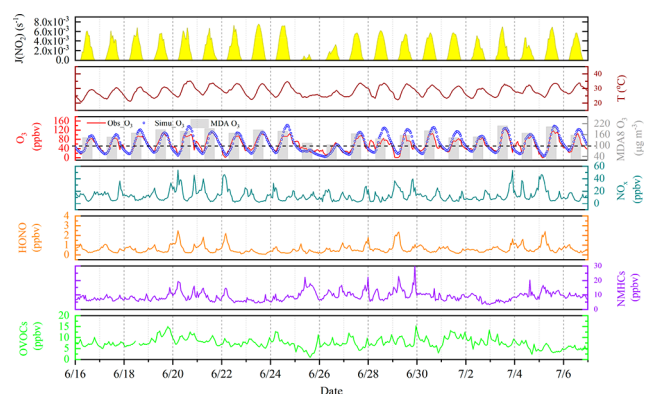


Figure 1. Time series of $\text{J}(\text{NO}_2)$, T, and typical gaseous pollutants (O_3 , NO_x , HONO, NMHCs, and OVOCs) during the sampling period.

daytime (6:00–18:00, UTC+8) average values at different O_3 pollution levels are listed in Table S1. Maximum daily average 8 h O_3 (MDA8 O_3) concentrations during the entire observation period all exceeded the Chinese ambient air quality first-grade standard ($100 \mu\text{g m}^{-3}$) and over half of them exceeded the second-grade standard ($160 \mu\text{g m}^{-3}$), revealing severe O_3 pollution during the summertime in Tai'an. The similar variation trend between O_3 and $\text{J}(\text{NO}_2)$ (Figure 1) as well as the obvious higher average value of $\text{J}(\text{NO}_2)$ at the levels of MDA8 O_3 exceeding $160 \mu\text{g m}^{-3}$ (Level-II) than at the levels of MDA8 O_3 in the range of 100 – $160 \mu\text{g m}^{-3}$ (Level-I) (Table S1) highlighted the importance of solar radiation for the photochemical formation of O_3 . Besides solar radiation, NO_x and VOCs as the key precursor species for O_3 also contributed greatly to O_3 production.^{4,5} However, high MDA8 O_3 concentration did not exactly correspond to the high daytime average values of the precursors (Table S1), which is likely due to the complex nonlinear interaction between O_3 and its precursors.^{6–8} Additionally, the average concentrations of HONO in the morning (6:00–9:00) were found to be greater at Level-II than those at Level-I (Figure S1), implying that atmospheric HONO might have a significant effect on O_3 production.

The O_3 production was thereafter analyzed using the observation-based model, and the simulated O_3 concentrations by the model with all the measured parameters as constraints were compared with the observation (Figure 1). As expected, the simulation results could well reproduce temporal variations in observed O_3 with a normalized mean bias (NMB) of 6.2%, confirming the credibility of the model simulation. The production and loss rates of O_3 were calculated based on the simulated concentrations of relevant species and the given reaction rate constants in the model. The O_3 production rate ($P(\text{O}_3)$) can be represented by the oxidation rates of NO to NO_2 by peroxy radicals,^{10,11} as expressed in eq 1. The O_3 loss rate ($L(\text{O}_3)$) can be quantified by summing O_3 photolysis (equivalent to the chemical removal of O^1D via its reaction with H_2O), the reactions of O_3 with OH, HO_2 and alkenes,

and the reaction of NO_2 with OH ,^{10,11} as described in eq 2. Then, the net production rates of O_3 ($\text{NP}(\text{O}_3)$) can be calculated via subtracting $\text{P}(\text{O}_3)$ by $\text{L}(\text{O}_3)$ (eq 3).

$$\text{P}(\text{O}_3) = k_{\text{HO}_2+\text{NO}}[\text{HO}_2][\text{NO}] + \sum k_{\text{RO}_{2,i}+\text{NO}}[\text{RO}_{2,i}][\text{NO}] \quad (1)$$

$$\begin{aligned} \text{L}(\text{O}_3) = & k_{\text{O}^1\text{D}+\text{H}_2\text{O}}[\text{O}^1\text{D}][\text{H}_2\text{O}] + k_{\text{OH}+\text{O}_3}[\text{OH}][\text{O}_3] \\ & + k_{\text{HO}_2+\text{O}_3}[\text{HO}_2][\text{O}_3] + k_{\text{alkenes}+\text{O}_3}[\text{alkenes}][\text{O}_3] \\ & + k_{\text{OH}+\text{NO}_2}[\text{OH}][\text{NO}_2] \end{aligned} \quad (2)$$

$$\text{NP}(\text{O}_3) = \text{P}(\text{O}_3) - \text{L}(\text{O}_3) \quad (3)$$

As shown in Figure S2, $\text{P}(\text{O}_3)$ was significantly greater than $\text{L}(\text{O}_3)$, resulting in daytime local accumulation of O_3 . The mean daytime reaction rates of NO with HO_2 and RO_2 were about 6.1 ppbv h^{-1} and 7.5 ppbv h^{-1} , accounting for $\sim 45\%$ and 55% of the total $\text{P}(\text{O}_3)$, respectively. The contribution proportions of the two dominant ways ($\text{NO}+\text{HO}_2$ and $\text{NO}+\text{RO}_2$) to $\text{P}(\text{O}_3)$ in Tai'an were different from those reported in other regions such as Xiamen (68% and 32%),¹² Baoding (57% and 43%),¹⁰ and Guangzhou (78% and 22%),⁴⁴ which was probably attributed to the emission differences in the precursors (e.g., OVOCs) of peroxy radicals (HO_2 and RO_2) in different areas. The fast elevation of $\text{P}(\text{O}_3)$ was found during 8:00–11:00, with diurnal average values increasing from 10 to 22 ppbv h^{-1} , implying the strong atmospheric oxidization capacity in the morning. Moreover, $\text{L}(\text{O}_3)$ was dominated by the reaction of NO_2 with OH ($\sim 41\%$), followed by the ozonolysis of alkenes ($\sim 32\%$) and O_3 photolysis ($\sim 12\%$) during the whole day.

Influence of HONO Concentration on the Production Rate of O_3

It has been acknowledged that the photolysis of HONO can trigger daytime atmospheric chemistry in the early morning and serve as the important or even dominant source for OH radicals, with a contribution of 20%–90%.^{13–15} The OH radicals can initiate the degradation of VOCs to produce RO_2 and HO_2 radicals which subsequently promote the efficient conversion of NO to NO_2 , leading to the accumulation of O_3 via NO_2 photolysis.⁵ However, the default mode (only the homogeneous reaction of NO and OH for HONO formation) in the box model tended to largely underestimate HONO levels (Figure 2a), with an average of 87% underprediction during the whole day, implying the existence of unknown strong sources of HONO. It should be noted that the simulated HONO was very close to the observed HONO during the entire observation period after the incorporation of the NO_2 heterogeneous mechanism in our recent study,²² which highlighted the importance of NO_2 uptake to HONO formation. Since this study mainly focused on the role of HONO in O_3 sensitive chemistry, the unknown HONO sources could be not further discussed in detail.

When the measured HONO concentrations were not input as constraints in the box model, the $\text{NP}(\text{O}_3)$ showed an obvious decrease ($\sim 19\%$) in the morning whereas it changed negligibly in the afternoon compared with HONO constraint (Figure 2b). Similar results were also found based on sensitivity tests with different degrees of HONO reduction in a previous study,¹⁸ which has been explained by the high HONO levels supplying the initiation of OH radicals in the early morning. In addition, the minimal influence of the

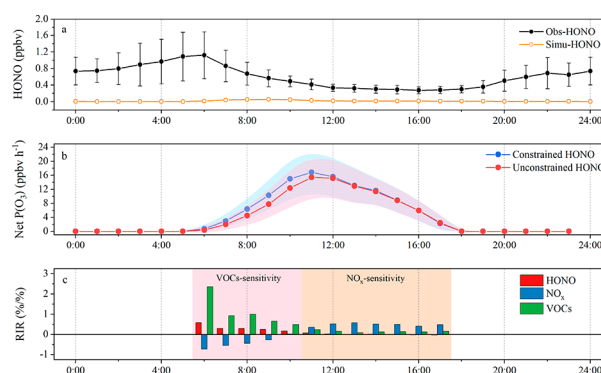


Figure 2. Diurnal trends of observed HONO and simulated HONO in the default box model (a), the variations of average diurnal net $\text{P}(\text{O}_3)$ with and without HONO constraint for the model (b), and the hourly RIR values of HONO, NO_x , and VOCs in the daytime (c).

unconstrained HONO on $\text{NP}(\text{O}_3)$ after 12:00 was mainly attributed to the low NO levels which were insufficient to meet RO_x and NO_x chemical cycles for O_3 production.

To further investigate the impact of HONO on O_3 production, the RIR,^{4,45} which is defined as the ratio of the decrease in $\text{NP}(\text{O}_3)$ to the decrease (20% in this study) in the concentrations of the specific species (X ; i.e., NO_x , VOCs or HONO), was calculated by eq 4 according to modeling results.

$$\text{RIR}_X = \frac{\Delta \text{NP}(\text{O}_3)_X / \text{NP}(\text{O}_3)_X}{\Delta C_X / C_X} \quad (4)$$

As shown in Figure 2c, the decrease in VOCs led to the positive RIR values during the daytime, with relatively high RIR values of 0.24–2.36 in the morning, indicating that the reduction of VOCs was an efficient way for O_3 pollution control, especially during the morning hours. Among all the VOCs, the RIR values of anthropogenic NMHCs (ANMHCs) were the highest, followed by biogenic VOCs (BVOCs) and OVOCs (Figure S3). However, the RIR values of NO_x were negative in the morning and then became positive in the afternoon, which was caused by the titration of NO_x to O_3 during VOC-sensitivity morning hours. Although HONO was not directly involved in the formation of O_3 , the decrease in HONO still resulted in the positive RIR values of 0.08–0.60 in the morning due to the dominant role of HONO in OH production. The RIR values of HONO were found to be about a factor of 3 less than those of VOCs, which was ascribed to the possibility that just approximately one-third of the OH radicals could react with VOCs to form RO_2 radicals.⁴⁶ Overall, not only NO_x and VOCs but also HONO have impacts on the local O_3 production.

Significance of Atmosphere HONO to the O_3 Sensitivity Regime

The average daily RIR values for VOCs and NO_x were also calculated with and without HONO constraint to examine the significance of atmospheric HONO to O_3 sensitive chemistry. As shown in Figure S4, the reductions of VOCs and NO_x tended to mitigate O_3 levels during the majority of the observed days, indicating that O_3 formation during the entire observation period was mainly in a mixed-sensitive regime. The unconstrained HONO in the default mode obviously increased the RIR values of VOCs but decreased the RIR values of NO_x , pushing O_3 production toward the VOC-sensitive regime. In particular, the RIR values of NO_x without

HONO constraint shifted from positive to negative over a few days (e.g., June 20 and 25). The change in the O₃ production sensitive regime without HONO constraint was determined by the reduction degree of HONO, and hence this shifting trend could be more significant in areas with the high HONO levels.

The impact of HONO on O₃-NO_x-VOC sensitivity was further analyzed using the visual isopleth diagrams which were generated from the EKMA mode, and the results are shown in Figure 3. It is clear that the ridge lines split the diagrams into

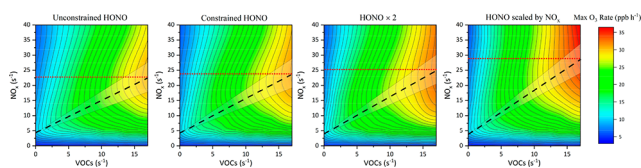


Figure 3. EKMA plots derived from multiple sensitivity tests in the box model. Unconstrained HONO: observed HONO not as a constraint for model input; Constrained HONO: observed HONO as a constraint for model input; HONO × 2: observed HONO scaled by a factor of 2 as a constraint for model input; HONO scaled by NO_x: HONO input increased or decreased with NO_x (assuming the ratio of HONO to NO_x is fixed). Note that the x-axis and y-axis represent the VOC and NO_x reactivities (s⁻¹), respectively. The red dashed lines were drawn to compare the gradient of the ridge lines among the different sensitivity tests.

two regimes, i.e., VOC-sensitive regime (upper) and NO_x-sensitive regime (lower). The yellowish shadowed area around the ridge line can be regarded as the mixed-sensitive regime of VOC and NO_x. As expected, the unconstrained HONO in the EKMA gave rise to slight decrease of the ridge line slope in comparison of HONO as constraints. For example, the NO_x reactivity reduced from 24 s⁻¹ to 22.5 s⁻¹ at VOCs reactivity of 17 s⁻¹, which was equivalent to lessening the NO_x-sensitive regime by nearly 7% at high VOCs level. Furthermore, with respect to the HONO scaled up by a factor of 2 as input, the unconstrained HONO could make the shrink percentage of the NO_x-sensitive regime become larger (~12%) in the EKMA, further underlining the significance of HONO to the O₃ sensitivity regime.

Along with the frequent occurrence of O₃ pollution in recent years for many Chinese cities, more and more diagnoses of O₃-NO_x-VOC sensitivity were performed using the box model (EKMA and RIR methods) based on the data obtained from local observation stations, in order to implement more precise control measures for alleviating O₃ pollution. However, the observed HONO data was not available in most local observation stations due to the difficulty and complexity of HONO measurement.⁴⁷ The unconstrained HONO in the default box model could cause a quite high level of underestimation in OH radicals and even incline the O₃ sensitive regime to VOCs, which could inevitably mislead policymakers into formulating efficient policies to control O₃ and improve air quality. Moreover, since HONO formation largely relies on concentrations of NO_x, it is unrealistic to only change NO_x but constrain HONO in the EKMA. If HONO is assumed to vary proportionally with NO_x in the EKMA, we will find a higher ridge line slope and a stronger NO_x-sensitive condition (Figure 3). The results suggest that emission control of NO_x should be also given much attention together with reducing VOC emissions for O₃ mitigation. Considering the significant role of HONO in diagnosing the sensitivity of O₃

production, HONO measurement should be added to conventional monitoring networks. Additionally, accurate concentrations of radicals such as OH, HO₂, and RO₂ can also cover the shortage of HONO measurement and help to provide more pivotal information about O₃ sensitive chemistry, and thus developing direct observation techniques for radicals is urgently needed.

■ ASSOCIATED CONTENT

SI Supporting Information

The Supporting Information is available free of charge at <https://pubs.acs.org/doi/10.1021/acsenvironau.2c00048>.

Additional details about the field campaign, model configurations and EKMA plots; supplementary diurnal variation of pollutants, hourly averaged RIR results and average values of key parameters during the field campaign (PDF)

■ AUTHOR INFORMATION

Corresponding Author

Yujing Mu – Research Center for Eco-Environmental Sciences, Chinese Academy of Sciences, Beijing 100085, China; University of Chinese Academy of Sciences, Beijing 100049, China; orcid.org/0000-0002-7048-2856; Email: yjmu@rcees.ac.cn

Authors

Pengfei Liu – Research Center for Eco-Environmental Sciences, Chinese Academy of Sciences, Beijing 100085, China; orcid.org/0000-0001-6237-3759

Chaoyang Xue – Research Center for Eco-Environmental Sciences, Chinese Academy of Sciences, Beijing 100085, China; orcid.org/0000-0001-6673-7716

Can Ye – Research Center for Eco-Environmental Sciences, Chinese Academy of Sciences, Beijing 100085, China; orcid.org/0000-0003-4350-0892

Chengtang Liu – Research Center for Eco-Environmental Sciences, Chinese Academy of Sciences, Beijing 100085, China

Chenglong Zhang – Research Center for Eco-Environmental Sciences, Chinese Academy of Sciences, Beijing 100085, China; University of Chinese Academy of Sciences, Beijing 100049, China

Jinhe Wang – Resources and Environment Innovation Research Institute, School of Municipal and Environmental Engineering, Shandong Jianzhu University, Ji'nan 250101, China

Yuanyuan Zhang – Research Center for Eco-Environmental Sciences, Chinese Academy of Sciences, Beijing 100085, China; University of Chinese Academy of Sciences, Beijing 100049, China

Junfeng Liu – Research Center for Eco-Environmental Sciences, Chinese Academy of Sciences, Beijing 100085, China; University of Chinese Academy of Sciences, Beijing 100049, China

Complete contact information is available at: <https://pubs.acs.org/10.1021/acsenvironau.2c00048>

Author Contributions

Y.M. conceived the study. P.L. performed the model simulations and wrote the manuscript. Y.M., C.Z., and J.L.

led the field campaign. C.X., C.Y., C.L., J.W., and Y.Z. provided observation data for the analysis.

Notes

The authors declare no competing financial interest.

ACKNOWLEDGMENTS

The authors thank Tai'an Municipal Ecological Environmental Bureau for logistical help. This work was financially supported by the National Natural Science Foundation of China (Grant No. 91544211, 41727805, 41905109, 21876186, and 21976108).

REFERENCES

- (1) Li, K.; Jacob, D. J.; Liao, H.; Zhu, J.; Shah, V.; Shen, L.; Bates, K. H.; Zhang, Q.; Zhai, S. A two-pollutant strategy for improving ozone and particulate air quality in China. *Nat. Geosci.* **2019**, *12*, 906–910.
- (2) Li, K.; Jacob, D. J.; Liao, H.; Shen, L.; Zhang, Q.; Bates, K. H. Anthropogenic drivers of 2013–2017 trends in summer surface ozone in China. *Proc. Natl. Acad. Sci. U. S. A.* **2019**, *116* (2), 422–427.
- (3) Wang, Y.; Gao, W.; Wang, S.; Song, T.; Gong, Z.; Ji, D.; Wang, L.; Liu, Z.; Tang, G.; Huo, Y.; Tian, S.; Li, J.; Li, M.; Yang, Y.; Chu, B.; Petäjä, T.; Kerminen, V.-M.; He, H.; Hao, J.; Kulmala, M.; Wang, Y.; Zhang, Y. Contrasting trends of PM_{2.5} and surface-ozone concentrations in China from 2013 to 2017. *Nat. Sci. Rev.* **2020**, *7* (8), 1331–1339.
- (4) Xue, L. K.; Wang, T.; Gao, J.; Ding, A. J.; Zhou, X. H.; Blake, D. R.; Wang, X. F.; Saunders, S. M.; Fan, S. J.; Zuo, H. C.; Zhang, Q. Z.; Wang, W. X. Ground-level ozone in four Chinese cities: precursors, regional transport and heterogeneous processes. *Atmos. Chem. Phys.* **2014**, *14* (23), 13175–13188.
- (5) Wang, T.; Xue, L.; Brimblecombe, P.; Lam, Y. F.; Li, L.; Zhang, L. Ozone pollution in China: A review of concentrations, meteorological influences, chemical precursors, and effects. *Sci. Total Environ.* **2017**, *575* (2017), 1582–1596.
- (6) Elshorbany, Y. F.; Kleffmann, J.; Kurtenbach, R.; Rubio, M.; Lissi, E.; Villena, G.; Gramscho, E.; Rickard, A. R.; Pilling, M. J.; Wiesen, P. Summertime photochemical ozone formation in Santiago, Chile. *Atmos. Environ.* **2009**, *43* (40), 6398–6407.
- (7) Louie, P. K. K.; Ho, J. W. K.; Tsang, R. C. W.; Blake, D. R.; Lau, A. K. H.; Yu, J. Z.; Yuan, Z.; Wang, X.; Shao, M.; Zhong, L. VOCs and OVOCs distribution and control policy implications in Pearl River Delta region, China. *Atmos. Environ.* **2013**, *76*, 125–135.
- (8) Shen, H.; Sun, Z.; Chen, Y.; Russell, A. G.; Hu, Y.; Odman, M. T.; Qian, Y.; Archibald, A. T.; Tao, S. Novel Method for Ozone Isopleth Construction and Diagnosis for the Ozone Control Strategy of Chinese Cities. *Environ. Sci. Technol.* **2021**, *55*, 15625–15636.
- (9) Liu, C.; Shi, K. A review on methodology in O₃-NO_x-VOC sensitivity study. *Environ. Pollut.* **2021**, *291*, 118249.
- (10) Tan, Z.; Lu, K.; Dong, H.; Hu, M.; Li, X.; Liu, Y.; Lu, S.; Shao, M.; Su, R.; Wang, H.; Wu, Y.; Wahner, A.; Zhang, Y. Explicit diagnosis of the local ozone production rate and the ozone-NO_x-VOC sensitivities. *Sci. Bull.* **2018**, *63* (16), 1067–1076.
- (11) Tan, Z.; Lu, K.; Jiang, M.; Su, R.; Dong, H.; Zeng, L.; Xie, S.; Tan, Q.; Zhang, Y. Exploring ozone pollution in Chengdu, southwestern China: A case study from radical chemistry to O₃-VOC-NO_x sensitivity. *Sci. Total Environ.* **2018**, *636*, 775–786.
- (12) Liu, T.; Hong, Y.; Li, M.; Xu, L.; Chen, J.; Bian, Y.; Yang, C.; Dan, Y.; Zhang, Y.; Xue, L.; Zhao, M.; Huang, Z.; Wang, H. Atmospheric oxidation capacity and ozone pollution mechanism in a coastal city of southeastern China: analysis of a typical photochemical episode by an observation-based model. *Atmos. Chem. Phys.* **2022**, *22* (3), 2173–2190.
- (13) Alicke, B.; Platt, U.; Stutz, J. Impact of nitrous acid photolysis on the total hydroxyl radical budget during the Limitation of Oxidant Production/Pianura Padana Produzione di Ozono study in Milan. *J. Geophys. Res.* **2002**, *107* (D22), LOP 9-1–LOP 9-17.
- (14) Kleffmann, J. Daytime sources of nitrous acid (HONO) in the atmospheric boundary layer. *ChemPhysChem* **2007**, *8* (8), 1137–44.
- (15) Xue, C.; Zhang, C.; Ye, C.; Liu, P.; Catoire, V.; Krysztofiak, G.; Chen, H.; Ren, Y.; Zhao, X.; Wang, J.; Zhang, F.; Zhang, C.; Zhang, J.; An, J.; Wang, T.; Chen, J.; Kleffmann, J.; Mellouki, A.; Mu, Y. HONO Budget and Its Role in Nitrate Formation in the Rural North China Plain. *Environ. Sci. Technol.* **2020**, *54* (18), 11048–11057.
- (16) Xue, C.; Ye, C.; Zhang, C.; Catoire, V.; Liu, P.; Gu, R.; Zhang, J.; Ma, Z.; Zhao, X.; Zhang, W.; Ren, Y.; Krysztofiak, G.; Tong, S.; Xue, L.; An, J.; Ge, M.; Mellouki, A.; Mu, Y. Evidence for Strong HONO Emission from Fertilized Agricultural Fields and its Remarkable Impact on Regional O₃ Pollution in the Summer North China Plain. *ACS Earth Space Chem.* **2021**, *5* (2), 340–347.
- (17) Zhang, J.; Lian, C.; Wang, W.; Ge, M.; Guo, Y.; Ran, H.; Zhang, Y.; Zheng, F.; Fan, X.; Yan, C.; Daellenbach, K. R.; Liu, Y.; Kulmala, M.; An, J. Amplified role of potential HONO sources in O₃ formation in North China Plain during autumn haze aggravating processes. *Atmos. Chem. Phys.* **2022**, *22* (5), 3275–3302.
- (18) Yang, Y.; Li, X.; Zu, K.; Lian, C.; Chen, S.; Dong, H.; Feng, M.; Liu, H.; Liu, J.; Lu, K.; Lu, S.; Ma, X.; Song, D.; Wang, W.; Yang, S.; Yang, X.; Yu, X.; Zhu, Y.; Zeng, L.; Tan, Q.; Zhang, Y. Elucidating the effect of HONO on O₃ pollution by a case study in southwest China. *Sci. Total Environ.* **2021**, *756*, 144127.
- (19) Xue, C. Substantially Growing Interest in the Chemistry of Nitrous Acid (HONO) in China: Current Achievements, Problems, and Future Directions. *Environ. Sci. Technol.* **2022**, *56*, 7375–7377.
- (20) Zhang, W.; Tong, S.; Jia, C.; Wang, L.; Liu, B.; Tang, G.; Ji, D.; Hu, B.; Liu, Z.; Li, W.; Wang, Z.; Liu, Y.; Wang, Y.; Ge, M. Different HONO Sources for Three Layers at the Urban Area of Beijing. *Environ. Sci. Technol.* **2020**, *54* (20), 12870–12880.
- (21) Liu, Y.; Lu, K.; Li, X.; Dong, H.; Tan, Z.; Wang, H.; Zou, Q.; Wu, Y.; Zeng, L.; Hu, M.; Min, K. E.; Kecorius, S.; Wiedensohler, A.; Zhang, Y. A Comprehensive Model Test of the HONO Sources Constrained to Field Measurements at Rural North China Plain. *Environ. Sci. Technol.* **2019**, *53* (7), 3517–3525.
- (22) Xue, C.; Ye, C.; Kleffmann, J.; Zhang, W.; He, X.; Liu, P.; Zhang, C.; Zhao, X.; Liu, C.; Ma, Z.; Liu, J.; Wang, J.; Lu, K.; Catoire, V.; Mellouki, A.; Mu, Y. Atmospheric measurements at Mt. Tai - Part II: HONO budget and radical (RO_x + NO₃) chemistry in the lower boundary layer. *Atmos. Chem. Phys.* **2022**, *22* (2), 1035–1057.
- (23) Kleffmann, J.; Becker, K. H.; Wiesen, P. Heterogeneous NO₂ conversion processes on acid surfaces: possible atmospheric implications. *Atmos. Environ.* **1998**, *32* (16), 2721–2729.
- (24) Wong, K. W.; Oh, H. J.; Lefer, B. L.; Rappenglück, B.; Stutz, J. Vertical profiles of nitrous acid in the nocturnal urban atmosphere of Houston, TX. *Atmos. Chem. Phys.* **2011**, *11* (8), 3595–3609.
- (25) VandenBoer, T. C.; Brown, S. S.; Murphy, J. G.; Keene, W. C.; Young, C. J.; Pszenny, A. A. P.; Kim, S.; Warneke, C.; de Gouw, J. A.; Maben, J. R.; Wagner, N. L.; Riedel, T. P.; Thornton, J. A.; Wolfe, D. E.; Dubé, W. P.; Öztürk, F.; Brock, C. A.; Grossberg, N.; Lefer, B.; Lerner, B.; Middlebrook, A. M.; Roberts, J. M. Understanding the role of the ground surface in HONO vertical structure: High resolution vertical profiles during NACHTT-11. *J. Geophys. Res.-Atmos.* **2013**, *118* (17), 10155–10171.
- (26) Tong, S. R.; Hou, S. Q.; Zhang, Y.; Chu, B. W.; Liu, Y. C.; He, H.; Zhao, P. S.; Ge, M. F. Exploring the nitrous acid (HONO) formation mechanism in winter Beijing: direct emissions and heterogeneous production in urban and suburban areas. *Faraday Discuss.* **2016**, *189* (2016), 213–230.
- (27) Wang, J.; Zhang, X.; Guo, J.; Wang, Z.; Zhang, M. Observation of nitrous acid (HONO) in Beijing, China: Seasonal variation, nocturnal formation and daytime budget. *Sci. Total Environ.* **2017**, *587–588* (2017), 350–359.
- (28) Zhang, W.; Tong, S.; Ge, M.; An, J.; Shi, Z.; Hou, S.; Xia, K.; Qu, Y.; Zhang, H.; Chu, B.; Sun, Y.; He, H. Variations and sources of nitrous acid (HONO) during a severe pollution episode in Beijing in winter 2016. *Sci. Total Environ.* **2019**, *648*, 253–262.
- (29) Wang, S.; Zhou, R.; Zhao, H.; Wang, Z.; Chen, L.; Zhou, B. Long-term observation of atmospheric nitrous acid (HONO) and its

implication to local NO₂ levels in Shanghai, China. *Atmos. Environ.* **2013**, *77*, 718–724.

(30) Bernard, F.; Cazaunau, M.; Grosselin, B.; Zhou, B.; Zheng, J.; Liang, P.; Zhang, Y.; Ye, X.; Daele, V.; Mu, Y.; Zhang, R.; Chen, J.; Mellouki, A. Measurements of nitrous acid (HONO) in urban area of Shanghai, China. *Environ. Sci. Pollut. Res.* **2016**, *23* (6), 5818–29.

(31) Chan, K. L.; Wang, S.; Liu, C.; Zhou, B.; Wenig, M. O.; Saiz-Lopez, A. On the summertime air quality and related photochemical processes in the megacity Shanghai, China. *Sci. Total Environ.* **2017**, *580*, 974–983.

(32) Ding, X.; Kong, L.; Du, C.; Zhanzakova, A.; Wang, L.; Fu, H.; Chen, J.; Yang, X.; Cheng, T. Long-range and regional transported size-resolved atmospheric aerosols during summertime in urban Shanghai. *Sci. Total Environ.* **2017**, *583*, 334–343.

(33) Li, S.; Song, W.; Zhan, H.; Zhang, Y.; Zhang, X.; Li, W.; Tong, S.; Pei, C.; Wang, Y.; Chen, Y.; Huang, Z.; Zhang, R.; Zhu, M.; Fang, H.; Wu, Z.; Wang, J.; Luo, S.; Fu, X.; Xiao, S.; Huang, X.; Zeng, J.; Zhang, H.; Chen, D.; Gligorovski, S.; Ge, M.; George, C.; Wang, X. Contribution of Vehicle Emission and NO₂ Surface Conversion to Nitrous Acid (HONO) in Urban Environments: Implications from Tests in a Tunnel. *Environ. Sci. Technol.* **2021**, *55*, 15616–15624.

(34) Qin, M.; Xie, P.; Su, H.; Gu, J.; Peng, F.; Li, S.; Zeng, L.; Liu, J.; Liu, W.; Zhang, Y. An observational study of the HONO-NO₂ coupling at an urban site in Guangzhou City, South China. *Atmos. Environ.* **2009**, *43* (36), 5731–5742.

(35) Liu, J.; Li, S.; Zeng, J.; Mekic, M.; Yu, Z.; Zhou, W.; Loisel, G.; Gandolfo, A.; Song, W.; Wang, X.; Zhou, Z.; Herrmann, H.; Li, X.; Gligorovski, S. Assessing indoor gas phase oxidation capacity through real-time measurements of HONO and NO_x in Guangzhou, China. *Environ. Sci.: Processes Impacts* **2019**, *21* (8), 1393–1402.

(36) Wu, T.; Zha, Q.; Chen, W.; Xu, Z.; Wang, T.; He, X. Development and deployment of a cavity enhanced UV-LED spectrometer for measurements of atmospheric HONO and NO₂ in Hong Kong. *Atmos. Environ.* **2014**, *95*, 544–551.

(37) Zha, Q.; Xue, L.; Wang, T.; Xu, Z.; Yeung, C.; Louie, P. K. K.; Luk, C. W. Y. Large conversion rates of NO₂ to HNO₂ observed in air masses from the South China Sea: Evidence of strong production at sea surface? *Geophys. Res. Lett.* **2014**, *41* (21), 7710–7715.

(38) Xu, Z.; Wang, T.; Wu, J.; Xue, L.; Chan, J.; Zha, Q.; Zhou, S.; Louie, P. K. K.; Luk, C. W. Y. Nitrous acid (HONO) in a polluted subtropical atmosphere: Seasonal variability, direct vehicle emissions and heterogeneous production at ground surface. *Atmos. Environ.* **2015**, *106*, 100–109.

(39) Jiang, Y.; Xue, L.; Shen, H.; Dong, C.; Xiao, Z.; Wang, W. Dominant Processes of HONO Derived from Multiple Field Observations in Contrasting Environments. *Environ. Sci. Technol. Lett.* **2022**, *9* (4), 258–264.

(40) Harris, G. W.; Carter, W. P. L.; Winer, A. M.; Pitts, J. N.; Platt, U.; Perner, D. Observations of nitrous acid in the Los Angeles atmosphere and implications for predictions of ozone-precursor relationships. *Environ. Sci. Technol.* **1982**, *16* (7), 414–419.

(41) Liu, P.; Zhao, X.; Zhang, C.; Chen, H.; Wang, J.; Xue, L.; Chen, J.; Mu, Y. Fine particle pH and its influencing factors during summer at Mt. Tai: Comparison between mountain and urban sites. *Atmos. Environ.* **2021**, *261*, 118607.

(42) Ye, C.; Xue, C.; Zhang, C.; Ma, Z.; Liu, P.; Zhang, Y.; Liu, C.; Zhao, X.; Zhang, W.; He, X.; Song, Y.; Liu, J.; Wang, W.; Sui, B.; Cui, R.; Yang, X.; Mei, R.; Chen, J.; Mu, Y. Atmospheric hydrogen peroxide (H₂O₂) at the foot and summit of Mt. Tai: Variations, sources and sinks, and implications for ozone formation chemistry. *J. Geophys. Res.-Atmos.* **2021**, *126* (15), No. e2020JD033975.

(43) Wolfe, G. M.; Marvin, M. R.; Roberts, S. J.; Travis, K. R.; Liao, J. The Framework for 0-D Atmospheric Modeling (FOAM) v3.1. *Geosci. Model Dev.* **2016**, *9* (9), 3309–3319.

(44) Tan, Z.; Lu, K.; Hofzumahaus, A.; Fuchs, H.; Bohn, B.; Holland, F.; Liu, Y.; Rohrer, F.; Shao, M.; Sun, K.; Wu, Y.; Zeng, L.; Zhang, Y.; Zou, Q.; Kiendler-Scharr, A.; Wahner, A.; Zhang, Y. Experimental budgets of OH, HO₂, and RO₂ radicals and implications

for ozone formation in the Pearl River Delta in China 2014. *Atmos. Chem. Phys.* **2019**, *19*, 7129–7150.

(45) Cardelino, C. A.; Chameides, W. L. An Observation-Based Model for Analyzing Ozone Precursor Relationships in the Urban Atmosphere. *J. Air Waste Manage. Assoc.* **1995**, *45* (3), 161–180.

(46) Whalley, L. K.; Slater, E. J.; Woodward-Massey, R.; Ye, C.; Lee, J. D.; Squires, F.; Hopkins, J. R.; Dunmore, R. E.; Shaw, M.; Hamilton, J. F.; Lewis, A. C.; Mehra, A.; Worrall, S. D.; Bacak, A.; Bannan, T. J.; Coe, H.; Percival, C. J.; Ouyang, B.; Jones, R. L.; Crilley, L. R.; Kramer, L. J.; Bloss, W. J.; Vu, T.; Kotthaus, S.; Grimmond, S.; Sun, Y.; Xu, W.; Yue, S.; Ren, L.; Acton, W. J. F.; Hewitt, C. N.; Wang, X.; Fu, P.; Heard, D. E. Evaluating the sensitivity of radical chemistry and ozone formation to ambient VOCs and NO_x in Beijing. *Atmos. Chem. Phys.* **2021**, *21* (3), 2125–2147.

(47) Xue, C.; Ye, C.; Ma, Z.; Liu, P.; Zhang, Y.; Zhang, C.; Tang, K.; Zhang, W.; Zhao, X.; Wang, Y.; Song, M.; Liu, J.; Duan, J.; Qin, M.; Tong, S.; Ge, M.; Mu, Y. Development of stripping coil-ion chromatograph method and intercomparison with CEAS and LOPAP to measure atmospheric HONO. *Sci. Total Environ.* **2019**, *646*, 187–195.